Dark to Bright Mode Conversion on Dipolar Nanoantennas: A Symmetry-Breaking Approach

Simone Panaro,[†] Adnan Nazir,[†] Carlo Liberale,[†] Gobind Das,[†] Hai Wang,[†,‡] Francesco De Angelis,[†] Remo Proietti Zaccaria,[†] Enzo Di Fabrizio,[§,⊥] and Andrea Toma*[,†]

[†]Istituto Italiano di Tecnologia, Via Morego 30, I-16163 Genova, Italy

[‡]College of Electronic Science and Engineering, Jilin University, 2699 Qianjin Street, Changchun 130012, China

[§]PSE and BESE Divisions, KAUST, King Abdullah University of Science and Technology, Thuwall, 23955-6900, Kingdom of Saudi Arabia

[⊥]BIONEM Lab, University of Magna Graecia, Campus S. Venuta, Germaneto, Viale Europa, I-88100 Catanzaro, Italy

Ⓢ *Supporting Information*

ABSTRACT: The excitation of plasmonic dark modes via a radiative channel is a phenomenon strongly hindered in the subwavelength regime. Recently, for achieving this purpose it has been proposed to exploit near-field interactions between radiating (bright) modes and lossless dark modes. However, this approach unveils challenging difficulties related to the excitation of dark modes through the near-field coupling with a bright mode. Here, it is experimentally and numerically shown how symmetry breaking applied to a nanoantenna dimer can conversely induce the excitation of plasmonic resonances, which play a key role for the dark modes' activation in more complex nanoassemblies. On the basis of this study, a T-shaped nanoantenna trimer has been introduced as an elemental unit for the energy transfer between bright and dark modes in plasmonic nanostructures. Finally, we implemented an analytical perturbative model to further investigate the plasmonic hybridization of subwavelength systems.

KEYWORDS: plamonics, nanostructures, near-field coupling, localized surface plasmon resonances, hybridized modes
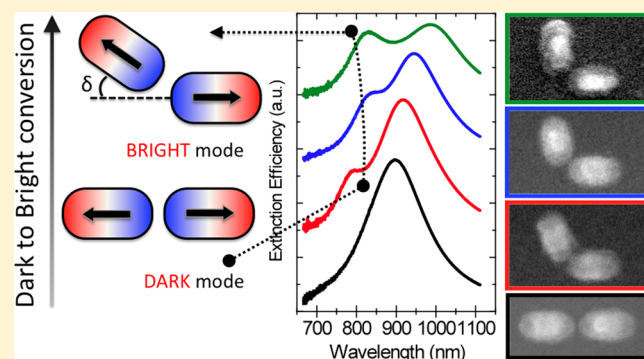
Considerable attention has been recently paid to the concept of plasmonic hybridization and in particular to the coupling between *bright* (radiating) and *dark* (nonradiating) modes supported by subwavelength systems.[1,2] A dark mode exchanging energy with a bright mode appears in far-field spectra as a narrow feature with remarkable implications in nonlinear plasmonics,[3] biosensing,[4] and metamaterial engineering.[5] However, dark modes are not easily excitable by means of radiative channels.[6] Recently, this difficulty has been overcome by the introduction of systems supporting high-order modes, which can be coupled to dipolar modes in the near-field interaction regime.[7] However, the complexity of such configurations implies stringent selections of the morphological parameters in order to match the energy transfer condition between bright and dark modes. A simpler approach for creating spectrally overlapped dark and bright modes consists in combining equivalent systems individually supporting dipolar plasmonic modes.[8,9]

In this perspective, rod-like nanoantennas are ideal building blocks for the construction of complex devices with *ad hoc* optoplasmonic responses.[10] In particular, the intense dipolar resonance (bright) of aligned nanoantenna dimers has been a matter of several studies for different applications in local field enhancement and far-field light manipulation.[11] Similarly, plasmonic dark modes have been studied in nanoantenna trimers under the excitation of radially polarized sources.[9] Considering the high potentialities of dark modes (e.g., longer lifetimes) in spite of their poor radiation coupling capability, a significant advance in this field would consist in applying the far-field properties of nanoantenna dimers inside trimer systems. Through exploiting the radiation efficiency presented by nanoantenna dimers in combination with the near-field properties of trimer nanosystems, it can be thought to obtain elemental units supporting Fano resonance by properly arranged rod-like nanoantennas.

Here we have investigated, both theoretically and experimentally, the activation in the far-field of a forbidden dipolar mode, by breaking the symmetry of a metallic nanoantenna dimer (i.e., by tilting one arm of the dimer; see Figure 1a). By adopting the bonding and antibonding description employed in the hybridization model,[12] we notice that the L-shaped configuration shows the most intense near-field-induced antibonding resonance. The application of these concepts to
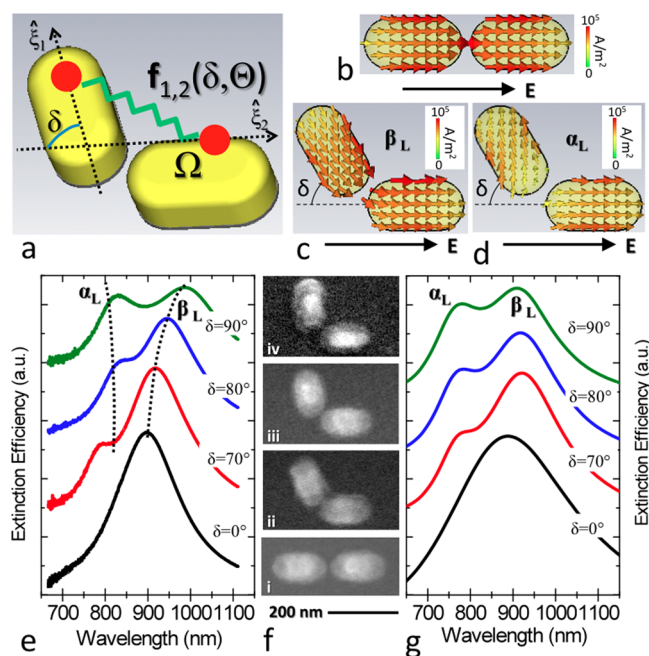
Figure 1. (a) Sketch of a tilted nanoantenna dimer. The two units forming the dimer have same length and width. (b−d) 2-D plots of charge current densities respectively for the bonding mode in aligned dimer and the bonding/antibonding modes in tilted dimer. (e, g) Experimental and simulated extinction spectra of nanoantenna dimers for different δ. (f) SEM images of dimers for tilt angles 0° (i), 70° (ii), 80° (iii), and 90° (iv) (single antenna sizes: length $l = 160$ nm, width $w = 80$ nm, height $h = 60$ nm, and interparticle gap 5 nm). In the figures, α and β stand for antibonding and bonding mode, respectively.

a T-shaped trimer has revealed the excitation of an antibonding dark mode. Finally, we have implemented a perturbative approach of the localized surface plasmons' (LSPs) interaction potential, in order to obtain a complete set of low-energy eigenmodes supported by nanoantenna assemblies.

Arrays of aligned and tilted Au nanoantenna dimers with a sub-10 nm interparticle gap have been fabricated on a CaF_2 (100) substrate by electron beam lithography (EBL) and physical vapor deposition[13] (Section 1, Supporting Information). The tilt angle δ (Figure 1) has been gradually increased moving from an aligned dimer (i) to an L-shaped dimer configuration (iv). Optical transmission spectroscopy in the visible and near-infrared region (Section 2, Supporting Information) has been performed on such arrays with a normal incident light source polarized parallel to the nontilted arm long

axis (Figure 1c). The experimental extinction spectra ($0° < \delta < 90°$) reveal a significant evolution in the line shape (Figure 1e). In fact, while for $\delta < 70°$ only a bonding peak is formed, for $\delta > 70°$ also an antibonding peak (Figure 1d) arises on the high-energy side of the spectrum. In order to confirm these results, near- and far-field simulations via Finite Integration Technique software[14] have been performed. For the aligned configuration ($\delta = 0°$) only the in-phase (bonding) bright mode occurs (Figure 1b), producing a broad extinction peak around 900 nm (black curve in Figure 1g). For tilted configurations, besides the in-phase mode (Figure 1c), an out-of-phase (antibonding) plasmonic mode arises characterized by charges that contemporarily move away from the center of the gap (Figure 1d). This resonance is clearly visible (around 770 nm) in the high-energy side of the far-field spectrum (Figure 1g). In far-field read-out, the radiative damping implies a spectral broadening of the resonance peaks. Therefore we needed a sub-10 nm interparticle gap in order to clearly distinguish the antibonding and bonding resonance peaks (Section 3, Supporting Information).

In order to provide a physical description of the origin of the antibonding mode, we have introduced a perturbative analytical model. Assuming that the LSP near-field interaction is much weaker than the energy of the unperturbed LSPs, we described the modes supported by the antenna assemblies as combinations of the single LSP modes supported by each antenna. Since the electromagnetic (EM) behavior of subwavelength systems can be well described in dipolar approximation,[15,16] the nanoantenna dimer has been treated as a mass-spring system in which the degrees of freedom are the charge displacements along each antenna main axis ($\hat{\xi}_1$ and $\hat{\xi}_2$ in Figure 1a). If we consider the electrostatic interaction between LSPs in terms of $f_{i,j}$, the equation of motion for the charge displacements results:

$$m^*\ddot{\xi}_i + m^*\gamma\dot{\xi}_i + \Omega\xi_i - \sum_{j\neq i} f_{i,j} = 0 \quad i, j = 1, 2 \tag{1}$$

where m^* is the effective mass of the charge distributions, γ is the internal damping affecting the motion of charges, and $\Omega = m^*\omega_0^2$ (ω_0 is the frequency of the unperturbed LSP). In linear approximation, eq 1 can be solved by diagonalizing the *potential interaction matrix* defined as $\overleftrightarrow{V} = \Omega I_{i,j} - \Theta\chi_{i,j}(\delta)$, where $I_{i,j}$ is Kroenecker's matrix, Ω is the LSP unperturbed energy parameter, Θ is the interaction parameter, and $\chi_{i,j}(\delta)$ is a function depending on the geometry (Section 4, Supporting Information). The matrix admits two eigenvectors, $\beta_L = (1/\sqrt{2})(\hat{\xi}_1,-\hat{\xi}_2)$ and $\alpha_L = (1/\sqrt{2})(\hat{\xi}_1,\hat{\xi}_2)$, which are respectively
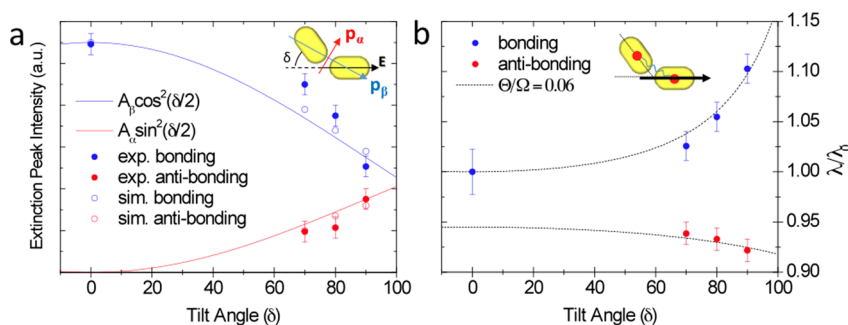

Figure 2. (a) Experimental (full dots) and simulated (empty dots) extinction efficiency referred to bonding (blue) and antibonding (red) peaks. The simulated values have been fitted with $\cos^2(\delta/2)$ and $\sin^2(\delta/2)$, respectively (continuous lines). (b) Positions of the experimental resonances of the hybridized modes, normalized to the resonant wavelength $\lambda_0 = 2\pi c/\omega_0$.[17]
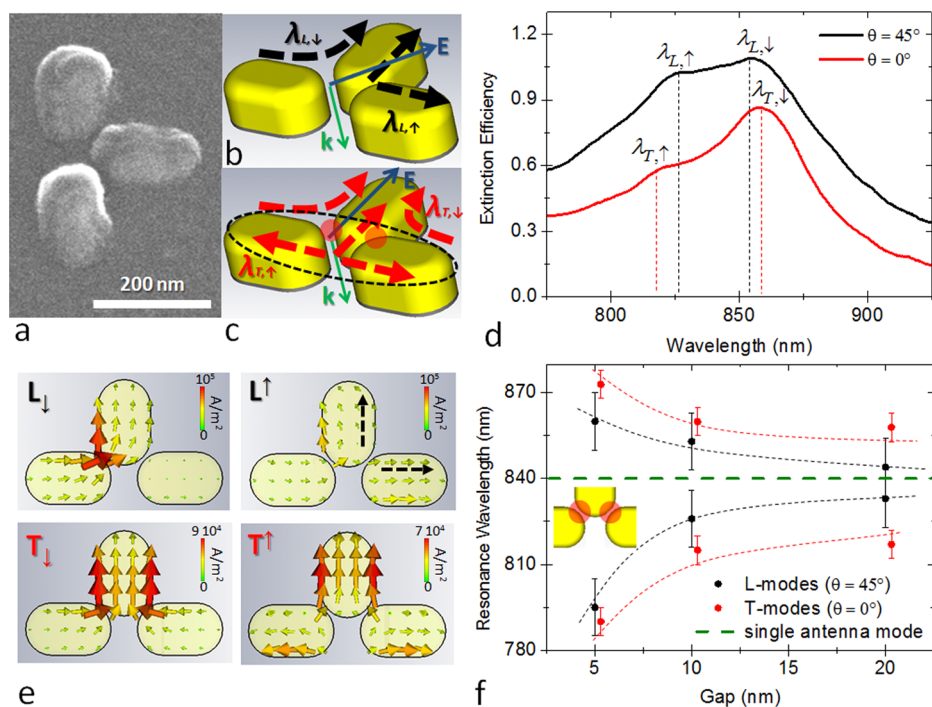
Figure 3. (a) SEM image of a single T-shaped antenna trimer with 10 nm interparticle gap. (b, c) Sketches presenting L- and T-type modes supported by a T-shape trimer. (d) Experimental extinction spectra of a 10 nm gap T-shape trimer for $\theta = \pm 45°$ (black line) and $\theta = 0°$ (red line) polarization angles, respectively. (e) 2-D plots of charge current densities for both the L- and T-type hybridized modes. (f) Resonant spectral positions of hybridized L-type modes (black dots) and T-type modes (red dots) supported by a T-shape trimer as a function of interparticle gap (the gap value corresponds to the two identical gaps between the orthogonal antennas and highlighted by red spots in the sketch in (f).

the in-phase and out-of-phase combinations of LSPs supported by the nanoantenna dimer (ξ_1, ξ_2 defined negative if directed toward the gap). In such an eigenbase the potential matrix reads

$$\vec{V} = \begin{pmatrix} \Omega - 2\Xi(\delta)\Gamma(\delta)\Theta & 0 \\ 0 & \Omega + 2\Xi(\delta)\Theta \end{pmatrix} \quad (2)$$

with $\Xi(\delta)$ and $\Gamma(\delta)$ being two positive functions increasing with the tilt angle δ. This fact confirms β_L and α_L as bonding ($\vec{V}_{1,1}$) and antibonding ($\vec{V}_{2,2}$) modes, respectively.

Both the eigenvectors and the eigenvalues obtained have remarkable implications in the extinction efficiency Q_{ext}. By considering that (i) under dipolar approximation Q_{ext} can be expressed in terms of dipolar momenta $\vec{P}_i$ and incident electric field amplitude $\vec{E}_0$[18] through $\sum_{j=\alpha,\beta}\vec{E}_0^* \cdot \vec{P}_j$[15] and (ii) the eigenvectors are proportional to the dipolar momentum $\vec{P}_j$, we can conclude that the extinction peaks associated to the bonding and antibonding modes are proportional to $\cos^2(\delta/2)$ and $\sin^2(\delta/2)$, respectively (Section 4, Supporting Information). In Figure 2a are plotted both the numerically simulated[14] and the modeled extinction peaks together with the experimental results, showing good agreement among the data. Furthermore, we can notice how the extinction peak of the antibonding mode α (red dots) increases with δ, according to the rise of the correspondent dipolar momentum (dark-to-bright conversion). In Figure 2b, the spread of the hybridized resonances for increasing δ reflects the influence of dimer arm rotation on the LSP coupling. Such behavior is confirmed in the theoretical model, by converting the eigenvalues of eq 2 into wavelengths as a function of δ. The resulting analytical curves depend on the ratio Θ/Ω, which expresses the interaction between the LSPs. By fitting the experimental resonant

wavelengths with our theoretical model, a small value of $\Theta/\Omega = 0.06$ (for gap size 5 nm) has been found, in good agreement with the perturbative assumption.

Such analysis highlights how the antibonding mode supported by an aligned dimer, dark for small δ, becomes bright (red curve in Figure 2a) by rotating one antenna. For $\delta = 90°$, the dimer assumes an L-shaped configuration and the excited LSP is induced exclusively via a near-field channel.

In order to extend such a concept to the near-field excitation of dark modes, a third antenna was added to an aligned dimer to form a T-shaped nanoassembly[8,9] (Figure 3b,c). This aspect confers to the system a new property, i.e., the possibility to excite an aligned-dimer dark mode[13] via the same near-field coupling phenomenon observed in the L-shaped nanoantenna dimer (Figure 3c). In fact the T-shaped trimer can be considered also as a superposition of L-shaped subelements, each of them supporting L-type modes (Figure 3b and Figure S5a in the Supporting Information).

Matrices of T-shaped nanoantennas with different gaps have been fabricated by means of EBL (Figure 3a) and optically characterized. We performed optical transmission spectroscopy with normally incident light polarized respectively at $\theta = 0°$, $\pm 45°$ angles with respect to the orthogonal antenna long axis (Figure 3d). From the $\theta = \pm 45°$ spectrum a clear bimodal line shape can be appreciated with two peaks centered around 825 nm ($L^\uparrow$) and 850 nm ($L_\downarrow$). Similarly, the $\theta = 0°$ polarization spectrum presents two peaks centered on 820 nm ($T^\uparrow$) and 860 nm ($T_\downarrow$). From simulated charge current distributions evaluated in $L^\uparrow$, $L_\downarrow$, $T^\uparrow$, and $T_\downarrow$, it is possible to attribute the four peaks to distinct plasmonic modes (Figure 3e). In particular, $T_\downarrow$ and $T^\uparrow$ involve all antenna arms and can be considered respectively as in-phase and out-of-phase combina-
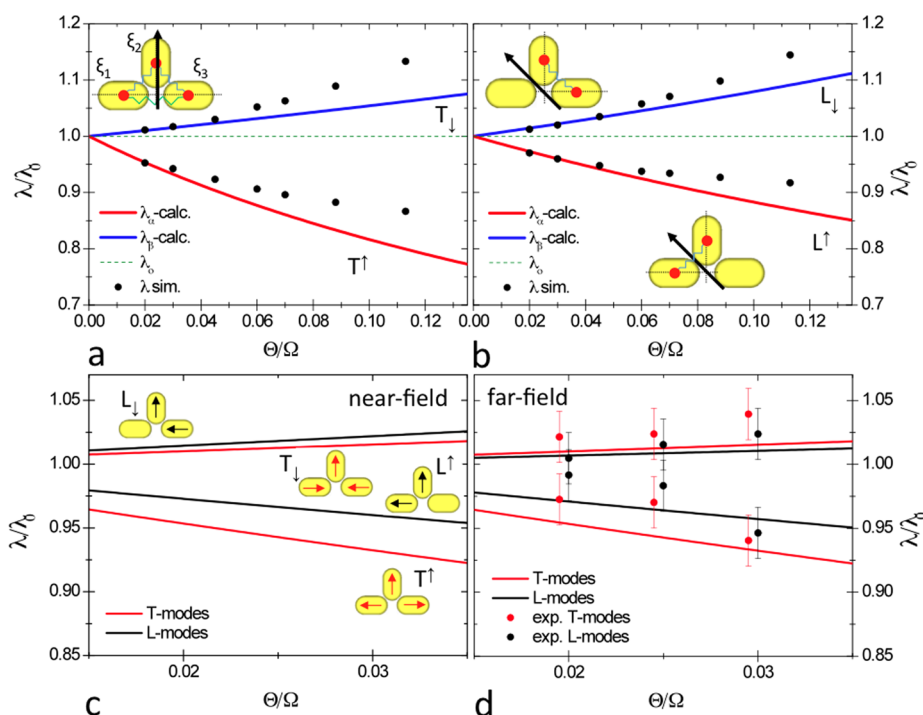
Figure 4. (a, b) Resonant wavelengths respectively of T-type and L-type modes normalized to the unperturbed resonant wavelength (λ_0) as a function of the Θ/Ω ratio (the continuous blue/red lines derive from the analytical analysis, and the black dots have been determined by numerical simulations). (c) Analytical curves for both L- and T-type resonant normalized modes in the perturbative interaction range. (d) Analytical curves for L- and T-type normalized resonant modes corrected on the basis of the radiation damping contribution (dots correspond to the normalized resonant positions collected from the experiment).

tions of an aligned-dimer dark mode with a single-antenna LSP (Figure S5b in the Supporting Information).

We collected the resonant wavelengths associated with these modes for different gaps (Figure 3f), noticing how, accordingly to the hybridization model,[12] the increase of the coupling strength, namely, reduction of the gap, widens the energy separation of both the L- and T-type modes with respect to the single-antenna resonance (green dashed line).

In the T-case, the potential matrix associated with the system reads

$$\vec{V}_T = \begin{pmatrix} \Omega + \left(1 + \dfrac{1}{\sqrt{2}}\right)\Theta & \dfrac{3}{\sqrt{2}}\Theta & \Theta \\[2ex] \dfrac{3}{\sqrt{2}}\Theta & \Omega + \sqrt{2}\,\Theta & \dfrac{3}{\sqrt{2}}\Theta \\[2ex] \Theta & \dfrac{3}{\sqrt{2}}\Theta & \Omega + \left(1 + \dfrac{1}{\sqrt{2}}\right)\Theta \end{pmatrix} \quad (3)$$

By solving the associated *secular equation*, this matrix has been diagonalized:

$$\vec{V}_T = \begin{pmatrix} \Omega + k_\eta^T\Theta & 0 & 0 \\[2ex] 0 & \Omega - k_\beta^T\Theta & 0 \\[2ex] 0 & 0 & \Omega + k_\alpha^T\Theta \end{pmatrix} \quad (4)$$

where k_η^T, k_β^T, and k_α^T are numerical coefficients defined as positive. The three eigenvectors associated with each eigenvalue are $\eta_T = (1/\sqrt{2})(\hat{\xi}_1, 0, -\hat{\xi}_3)$, $\beta_T \propto (-\hat{\xi}_1, \varepsilon_\beta \hat{\xi}_2, -\hat{\xi}_3)$, and $\alpha_T \propto (\hat{\xi}_1, \varepsilon_\alpha \hat{\xi}_2, \hat{\xi}_3)$, respectively, with ε_β and ε_α being positive coefficients. The first and third components of the eigenvectors

correspond to the aligned-dimer LSPs, while the second one is related to the single orthogonal arm (sketch in Figure 4a). Accordingly, the eigenstate denoted with β_T corresponds to the bonding mode defined as $T_\downarrow$, while the eigenstate indicated as α_T corresponds to the antibonding mode $T^\uparrow$ (Figure 3e).

More in general, the quantities $\Omega - k_\beta^L\Theta$, $\Omega + k_\alpha^L\Theta$, $\Omega - k_\beta^T\Theta$, and $\Omega + k_\alpha^T\Theta$ (where $k_\beta^L = 2\Xi(90°)\,\Gamma(90°)$ and $k_\alpha^L = 2\Xi(90°)$) can be respectively associated with the $L_\downarrow$, $L^\uparrow$, $T_\downarrow$, and $T^\uparrow$ hybridized modes (Figure 3b,c). For evaluating the validity range of our model, the analytical resonance wavelengths (Figure 4a,b) have been compared with the values obtained by near-field simulations, varying the interaction term Θ (the near-field resonances have been calculated within the gap regions highlighted by red spots in the sketch of Figure 3f, on a plane that passes through the center of the structures). The comparison between simulated (black dots) and analytical results (red and blue lines) highlights a good agreement between model and simulations when $\Theta/\Omega < 5\%$.

Considering L- and T-type resonant wavelengths in the perturbative interaction regime (Figure 4c), $T^\uparrow$ and $L_\downarrow$ modes appear as the most unfavorable and favorable configurations, respectively. Such attributions are referred to the electrostatic energy accumulated in the gap region of the T-shaped trimer during an optical cycle. Considering the total charge induced within the gap region, $T^\uparrow$ and $L_\downarrow$ are the modes, which respectively require the highest and the lowest amount of energy for being excited. Interestingly, when the far-field (Figure 3d) and near-field (Figure 4c) behaviors are compared, a different spectral position/ordering of the resonances can be noticed. This near-/far-field shifting is well recognized as a consequence of the radiative damping of bright modes.[19] In order to properly compare the analytical and experimental

results, we numerically quantified the shifts between near- and far-field resonant wavelengths,[13] permitting the correction of the analytical curves (Figure 4d). By reporting the measured far-field resonant wavelengths on the damping-corrected curves, we observed the agreement of the analytical model with the experimental results (Figure 4d).

In conclusion, we have shown how the symmetry breaking of a nanoantenna dimer can induce dark-to-bright conversion of a dipolar antibonding mode. This approach represents a further step in light manipulation at the nanoscale, paving the way toward the realization of all-optical switches[2] based on the dark-to-bright conversion. Exploiting the near-field coupling which triggers L-type modes, we conceived a T-shaped nanoantenna trimer presenting the excitation of an antibonding dark mode via the near-field coupling with a dipolar bright mode. In order to strengthen the physical interpretation of the experimental results, a theoretical model for subwavelength systems has been implemented under perturbative approximation. In this way we derived the complete set of low-energy hybridized plasmonic modes responsible for the spectral behavior of the plasmonic systems hereby introduced.

■ ASSOCIATED CONTENT

Ⓢ Supporting Information

This material is available free of charge via the Internet at http://pubs.acs.org.

■ AUTHOR INFORMATION

Corresponding Author

*E-mail: andrea.toma@iit.it.

Notes

The authors declare no competing financial interest.

■ REFERENCES

(1) Lassiter, J. B.; Sobhani, H.; Knight, M. W.; Mielczarek, W. S.; Nordlander, P.; Halas, N. J. Designing and deconstructing the Fano lineshape in plasmonic nanoclusters. *Nano Lett.* **2012**, *12*, 1058−1062.

(2) Chang, W.-S.; Lassiter, J. B.; Swanglap, P.; Sobhani, H.; Khatua, S.; Nordlander, P.; Halas, N. J.; Link, S. A plasmonic Fano switch. *Nano Lett.* **2012**, *12*, 4977−4982.

(3) Kauranen, M.; Zayats, A. V. Nonlinear plasmonics. *Nat. Photonics* **2012**, *6*, 737−748.

(4) Anker, J. N.; Hall, W. P.; Lyandres, O.; Shah, N. C.; Zhao, J.; Van Duyne, R. P. Biosensing with plasmonic nanosensors. *Nat. Mater.* **2008**, *7*, 442−453.

(5) Luk'yanchuk, B.; Zheludev, N. I.; Maier, S. A.; Halas, N. J.; Nordlander, P.; Giessen, H.; Chong, C. T. The Fano resonance in plasmonic nanostructures and metamaterials. *Nat. Mater.* **2010**, *9*, 707−715.

(6) Mukherjee, S.; Sobhani, H.; Lassiter, J. B.; Bardhan, R.; Nordlander, P.; Halas, N. J. Fanoshells: Nanoparticles with Built-in Fano Resonances. *Nano Lett.* **2010**, *10*, 2694−2701.

(7) Habteyes, T. G.; Dhuey, S.; Cabrini, S.; Schuck, P. J.; Leone, S. R. Theta-Shaped Plasmonic Nanostructures: Bringing "Dark" Multipole Plasmon Resonances into Action via Conductive Coupling. *Nano Lett.* **2011**, *11*, 1819−1825.

(8) Zhang, S.; Genov, D. A.; Wang, Y.; Liu, M.; Zhang, X. Plasmon-induced transparency in metamaterials. *Phys. Rev. Lett.* **2008**, *101*, 047401.

(9) Gómez, D. E.; Teo, Z. Q.; Altissimo, M.; Davis, T. J.; Earl, S.; Roberts, A. The Dark Side of Plasmonics. *Nano Lett.* **2013**, *13*, 3722−3728.

(10) Yu, N. F.; Genevet, P.; Kats, M. A.; Aieta, F.; Tetienne, J. P.; Capasso, F.; Gaburro, Z. Light propagation with phase discontinuities: generalized laws of reflection and refraction. *Science* **2011**, *334*, 333−337.

(11) Biagioni, P.; Huang, J. S.; Hecht, B. Nanoantennas for visible and infrared radiation. *Rep. Prog. Phys.* **2012**, *75*, 024402.

(12) Nordlander, P.; Oubre, C.; Prodan, E.; Li, K.; Stockman, M. I. Plasmon hybridizaton in nanoparticle dimers. *Nano Lett.* **2004**, *4*, 899−903.

(13) Neubrech, F.; Weber, D.; Katzmann, J.; Huck, C.; Toma, A.; Di Fabrizio, E.; Pucci, A.; Hartling, T. Infrared optical properties of nanoantenna dimers with photochemically narrowed gaps in the 5 nm regime. *ACS Nano* **2012**, *6*, 7326−7332.

(14) *Finite Integration Technique*; CST, Computer Simulation Technology: Darmstadt, Germany, 2010.

(15) Yang, W. H.; Schatz, G. C.; Vanduyne, R. P. Discrete dipole approximation for calculating extinction and Raman intensities for small particles with arbitrary shapes. *J. Chem. Phys.* **1995**, *103*, 869−875.

(16) Bowen, P. T.; Driscoll, T.; Kundtz, N. B.; Smith, D. R. Using a discrete dipole approximation to predict complete scattering of complicated metamaterials. *New J. Phys.* **2012**, *14*, 033038.

(17) The bonding and antibonding resonant wavelengths have been normalized to the bonding resonance wavelength of the dimer for $\delta = 0°$. In fact, in the oscillator model, the single-antenna mode and the aligned-dimer bonding mode are degenerate.[11]

(18) Bohren, C. F.; Huffman, D. R. *Absorption and Scattering of Light by Small Particles*; Wiley: New York, 1983.

(19) Alonso-Gonzalez, P.; Albella, P.; Neubrech, F.; Huck, C.; Chen, J.; Golmar, F.; Casanova, F.; Hueso, L. E.; Pucci, A.; Aizpurua, J.; Hillenbrand, R. Experimental verification of the spectral shift between near- and far-field peak intensities of plasmonic infrared nanoantennas. *Phys. Rev. Lett.* **2013**, *110*, 203902.